International Journal of Mechanical, Industrial and Aerospace Sciences
ISSN: 2517-9950
Vol:6, No:11, 2012

Chaotic Oscillations of Diaphragm Supported by Nonlinear Springs with Hysteresis

M. Sasajima, T. Yamaguchi, Y. Koike, and A. Hara

***Abstract*—**This paper describes vibration analysis using the finite element method for a small earphone, especially for the diaphragm shape with a low-rigidity. The viscoelastic diaphragm is supported by multiple nonlinear concentrated springs with linear hysteresis damping. The restoring forces of the nonlinear springs have cubic nonlinearity. The finite elements for the nonlinear springs with hysteresis are expressed and are connected to the diaphragm that is modeled by linear solid finite elements in consideration of a complex modulus of elasticity. Further, the discretized equations in physical coordinates are transformed into the nonlinear ordinary coupled equations using normal coordinates corresponding to the linear natural modes. We computed the nonlinear stationary and non-stationary responses due to the internal resonance between modes with large amplitude in the nonlinear springs and elastic modes in the diaphragm. The non-stationary motions are confirmed as the chaos due to the maximum Lyapunov exponents with a positive number. From the time histories of the deformation distribution in the chaotic vibration, we identified nonlinear modal couplings.

***Keywords*—**Nonlinear Vibration, Finite Element Method, Chaos ,Small Earphone.

I. Introduction

THE small diaphragm typically used in small earphones usually vibrates with complicated deformation of the entire diaphragm body. The rigidity of this type of diaphragm can be adjusted by changing the dimensional values of the design parameters such as the diameter, shape of the center dome, and shape of the helical channel of the periphery known as corrugation. However, because of the nonlinear load-displacement relation of the diaphragm, nonlinear vibrations are expected. The rigidity of a part of the diaphragm is not uniform because a lead wire, used for conducting electricity to the electric conductor, is glued to the back of the diaphragm; therefore, the out-plane displacement of the diaphragm in the circumferential direction could become uneven. Furthermore, although the displacement of the diaphragm is usually kept small to suppress the nonlinear vibrations owing to an emphasis on the linearity of the vibration amplitude and the uniformity of the excitation force, to obtain the necessary output from the miniaturized units containing diaphragms, it has recently become necessary to increase the vibration amplitude with respect to the diameter of the diaphragm. Depending on the vibration modal coupling characteristics, both transient and chaotic vibrations are expected to occur. Hence, the vibration analysis of small-sized earphone diaphragms with nonlinearity has become very important. Research on the vibration characteristics of systems containing nonlinear concentrated springs has been conducted. For example, Kondo proposed a high-speed stability criterion method concerning the forced vibration of a structure connected with nonlinear supporting beams [1]. Shaw conducted a nonlinear analysis of a system involving a beam with simple supports at two ends supported by a nonlinear concentrated spring in the middle [2]. On the other hand, Yamaguchi analyzed the coupled vibration of a system involving a block-shaped structure supported by a nonlinear concentrated spring, by using linear finite elements to model the elastic body [3], [4]. Yamaguchi proposed a high-speed computation method for a response that introduces a normal coordinate corresponding to a linear vibration mode, and expanded this method to formulate a viscoelastic block connected to a nonlinear concentrated spring with linear hysteresis damping in the restoring force [5]. Moreover, a considerable amount of research has been conducted on the nonlinear vibration characteristics of systems consisting of an elastic structure and nonlinear concentrated springs and the chaotic vibration phenomena of plates and shells due to internal resonance [6]–[8]. However, nonlinear response analyses of the transient and chaotic vibrations of small earphone diaphragms have not yet been carried out. In the present study, the characteristics of nonlinear springs were identified by an actual measurement of the load-displacement relationship of the diaphragm, and the soft portion at the periphery of the diaphragm was modeled by using several nonlinear concentrated springs with hysteresis. The resonance response of the center section of the diaphragm supported with these nonlinear concentrated springs was analyzed. Because the out-plane displacement of the diaphragm is dominated by the effect of the deformation of the nonlinear springs, the geometric nonlinearity of the center section of the diaphragm was not considered. The precision of the numerical computation in comparison to that of the actual examination model was verified in a previous study. The steady-state and transient vibration responses were analyzed by applying cyclic external excitation forces to the system. Furthermore, from the time history of the response, the largest Lyapunov exponent was calculated, and it was verified that the transient response was a chaotic vibration [9].

M. Sasajima is with the Strategic Development Division, Foster electric Co., Ltd., 196-8550, 512 Miyazawa-cho, Akishima, Tokyo, Japan (phone: 042-546-2445; fax: 042-546-2340; e-mail: sasajima@ foster.co.jp).

T. Yamaguchi is with the Department of Mechanical System Engineering, Gunma University, 376-8515, 1-5-1, Tenjin-cho, Kiryu, Gunma, Japan (e-mail: yamagme3@gunma-u.ac.jp).

Y. Koike is with the Strategic Development Division, Foster electric Co., Ltd, 196-8550, 512 Miyazawa-cho, Akishima, Tokyo, Japan (phone: 042-546-2445; fax: 042-546-2340; e-mail: koike@ foster.co.jp).

A. Hara is with the Strategic Development Division, Foster electric Co., Ltd, 196-8550, 512 Miyazawa-cho, Akishima, Tokyo, Japan (phone: 042-546-2445; fax: 042-546-2340; e-mail: ahara@ foster.co.jp).

II. Simulation Model

Fig. 1 shows the model used in the simulation. The shape of the section near the central portion of the diaphragm and the electric conductor vibrating in conjunction with the diaphragm are modeled by using finite elements.

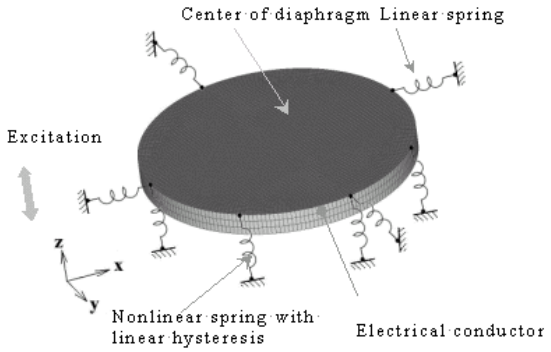

Fig. 1 Simulation model

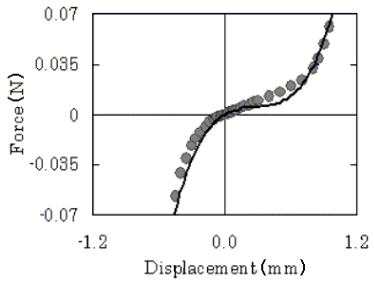

Fig. 2 Restoring force of nonlinear concentrated springs
(●: Experiment —: Approximation)

The center section has a diaphragm thickness of 10 μm, a diameter of 7.0 mm, and a height of 1.0 mm. The densities of the diaphragm and electric conductor are 6.12×10^2 kg/m^3 and 8.78×10^3 kg/m^3, respectively. To consider the compliance of the back air chamber, an equivalent elastic element is introduced at the back of the diaphragm. The origin of the model is set at the center of the bottom surface of the x-y plane of the diaphragm, and the excitation direction is along the z direction. Response points are set around the periphery of the central part of the center section. The center section and the electric conductor are modeled by the isoparametric solid elements of eight nodes [10]. Concentrated springs are used for modeling the very soft portion around the outer edge of the electric conductor of the diaphragm, and three concentrated springs are placed at each node at the circumference of the diaphragm center section in the x, y, and z directions. The concentrated spring in the z direction is a nonlinear concentrated spring. Fig. 2 shows the static load-displacement curve of the nonlinear concentrated spring. The dynamic analysis considers hysteresis with a complex spring having a hardening spring characteristic of the restoring force. The Young's modulus of the diaphragm center section is 3.07 GPa, and the Poisson's ratio is 0.29. The electric conductor has an equivalent Young's modulus of 33.0 GPa , considering the resin adhesive layer. The spring constants of the nonlinear springs are as follows: $\bar{\gamma}_{1mz} = 4.54 \times 10^{-3} N/mm$, $\gamma_{2mz} = 1.53 \times 10^{-2} N/mm^2$, and $\gamma_{3mz} = 1.82 \times 10^{-2} N/mm^3$. Further, the material loss factor η_s is 0.01. The spring constants in the x and y directions are $\gamma_{mx} = \gamma_{my} = 4.54 \times 10^{-3} N/mm$. A material loss factor η_s of the same value as that of the nonlinear spring in the z direction was given.

III. Analysis Method

As shown in Fig. 1, a case in which the center section of the diaphragm is supported with multiple nonlinear concentrated springs is considered. The discretization equation of the finite elements of this system is calculated.

A. Discretization Equations of Nonlinear Concentrated Springs

The force at the node of the nonlinear concentrated spring is expressed as $R_{mz} = \gamma_{1mz} U_{mz} + \gamma_{2mz} U_{mz}^{\ 2} + \gamma_{3mz} U_{mz}^{\ 3}$, (m = 1, 2, 3, …). U_{mz} is the z direction displacement of the node corresponding to the installation point of the nonlinear concentrated spring to the diaphragm center section. The relationship between R_{mz} and U_{mz} is described using a matrix, and the following formula is obtained:

$$\{R_m\} = [\bar{\gamma}_{1m}]\{U_s\} + \{\bar{d}_m\} \quad (1)$$

where

$\{R_m\} = \{\gamma_{mx}, \gamma_{my}, \gamma_{mz}\}^T$,

$\{U_s\} = \{U_{mx}, U_{my}, U_{mz}\}^T$,

$\{\bar{d}_m\} = \{0, 0, \gamma_{2mz} U_{mz}^{\ 2} + \gamma_{3mz} U_{mz}^{\ 3}\}^T$.

Furthermore, $\gamma_{mx} = \gamma_{my} = 0$. $\{R_m\}$ is the restoring force vector of the *m* nonlinear concentrated spring, $\{U_s\}$ is the node displacement vector, $[\bar{\gamma}_{1m}]$ is the linear complex stiffness matrix, and $\{\bar{d}_m\}$ is the nonlinear restoring force vector. Linear hysteresis damping is introduced into the concentrated spring by setting $\gamma_{1mz} = \bar{\gamma}_{1mz}(1 + j\eta_s)$. Here, $\bar{\gamma}_{1mz}$ is the real number part of γ_{1mz} , η_s is the material loss factor corresponding to the linear restoring force of the concentrated spring, and j is an imaginary unit.

B. Discretization Equations of Center Section of Viscoelastic Diaphragm

The center section of the diaphragm is partitioned into three-dimensional finite elements. Assuming that the deformation of the finite elements is small, we use ordinary linear three-dimensional elements. The displacement vector in each element is $\{U_d\} = \{U_x, U_y, U_z\}^T$, which can be approximated with node displacement vector $\{U_e\}$ and shape

function $[N]^T$ according to the following equation:

$$\{U_d\} = [N]^T \{U_e\} \tag{2}$$

The relation between the stress vector $\{\sigma\} = \{\sigma_x \quad \sigma_y \quad \sigma_z \quad \tau_{xy} \quad \tau_{yz} \quad \tau_{zx}\}^T$ and the strain vector $\{\varepsilon\} = \{\varepsilon_x \quad \varepsilon_y \quad \varepsilon_z \quad \gamma_{xy} \quad \gamma_{yz} \quad \gamma_{zx}\}^T$ is converted into the following relation:

$$\{\sigma\} = [D]\{\varepsilon\} \tag{3}$$

$[D]$ is a matrix consisting of the modulus of elasticity E_e a nd Poisson's ratio ν_e. The relation between the displacement vector $\{U_d\}$ and the strain vector $\{\varepsilon\}$ can then be expressed as follows:

$$\{\varepsilon\} = [A]\{U_d\} = [A][N]^T \{U_e\} = [B]\{U_e\} \tag{4}$$

From (2) and (4), by calculating the work based on the strain energy, kinetic energy, and external force of the element and by solving the discretization equation of the section center of the diaphragm excluding the spring elements on the basis of the virtual work principle, we can express the mass matrix of the center section of the diaphragm $[M_f]$, the complex stiffness matrix $[K_f]$, the node displacement vector $\{U_f\}$, and the nodal force vector $\{F_f\}$ as the following relation. • indicates time differentiation.

$$[M_f]\{\ddot{U}_f\} = -[K_f]\{U_f\} + \{F_f\} \tag{5}$$

C. Discretization Equations of System Connecting Viscoelastic Diaphragm Center Section and Nonlinear Spring

The nodal force due to the nonlinear concentrated spring in the z direction $\{R_m\}$ is added to the nodal force of the node that connects the diaphragm center section. From this, we obtained the discretization equation of the entire system.

$$[M]\{\ddot{U}\} = -[K]\{U\} - \{\hat{d}\} + \{F\} \tag{6}$$
$$\{\hat{d}\} = \sum_m \{\hat{d}_m\}$$

$[M]$, $[K]$, $\{U\}$, and $\{F\}$ are the mass matrix, complex stiffness matrix, nodal displacement vector, and nodal force vector, respectively. $\{\hat{d}_m\}$ corrects the size $\{\overline{d}_m\}$ of the vector of the nonlinear restoring force in (1) as the size of the entire system.

D. Approximate Computation of Modal Damping

In (6), the terms of the external force and the nonlinear restoring force are {0}. Assuming $\{U\} = \{\phi\}e^{j\omega t}$ (t: time), we obtain the following eigenvalue problem equation:

$$\sum_{e=1}^{e\max} ([K_R]_e (1 + j\eta_e) - (\omega^{(i)})^2 (1 + j\eta_{tot}^{(i)})[M]_e)\{\phi^{(i)}\} = \{0\} \tag{7}$$

where (i) denotes the mode number of the vibration; $(\omega^{(i)})^2$, the real part of the complex eigenvalue; $\{\phi^{(i)}\}$, the complex normal mode; and $\eta_{tot}^{(i)}$, the modal loss factor. A normalized factor, the material damping coefficient η_e $(e = 1,2,3,...e_{\max})$ with respect to the maximal in all the elements $\eta_{\max}$, β_e is defined as follows:

$$\beta_e = \eta_e / \eta_{\max}, \beta_e \le 1 \tag{8}$$

Here, assuming $\eta_{\max} << 1$, introducing a small quantity $\mu = j\eta_{\max}$, and expanding the solution of (7) asymptotically lead to the following equations:

$$\{\phi^{(i)}\} = \{\phi^{(i)}\}_0 + \mu\{\phi^{(i)}\}_1 + \mu^2\{\phi^{(i)}\}_2 + ,... \tag{9}$$
$$(\omega^{(i)})^2 = (\omega_0^{(i)})^2 + \mu^2(\omega_2^{(i)})^2 + \mu^4(\omega_4^{(i)})^2 + ,... \tag{10}$$
$$j\eta_{tot}^{(i)} = \mu\eta_1^{(i)} + \mu^3\eta_3^{(i)} + \mu^5\eta_5^{(i)} + \mu^7\eta_7^{(i)} + ,... \tag{11}$$

Because $\beta_e \le 1$ and $\eta_{\max}\beta_e << 1$, $\mu\beta_e$ is also a small quantity, the same as μ. Further, $\{\phi^{(i)}\}_0$, $\{\phi^{(i)}\}_1$,… with $(\omega_0^{(i)})^2$, $(\omega_2^{(i)})^2$,…, and $\eta_1^{(i)}$, $\eta_3^{(i)}$,… are real numbers. Substituting (9)–(11) and (7) and rearranging the terms of μ^0 and μ^1 yields the following equation:

$$\eta_{tot}^{(i)} = \sum_{e=1}^{e\max} \left(\eta_e S_e^{(i)}\right), \tag{12}$$
$$S_e^{(i)} = \{\phi^{(i)}\}_0^T [K_R]_e \{\phi^{(i)}\}_0 / \sum_{e=1}^{e\max} \left(\{\phi^{(i)}\}_0^T [K_R]_e \{\phi^{(i)}\}_0\right)$$

$S_e^{(i)}$ is the share of the strain energy (strain energy of element e/strain energy of all systems) of each element under the condition of the deformation of the i-degree vibration mode. $\{\phi^{(i)}\}_0$ denotes the real normal mode. From (12), we can calculate the approximate modal loss factor $\eta_{tot}^{(i)}$ using the sum of the product of the material loss factor η_e and the share of the strain energy $S_e^{(i)}$ of all elements. $\eta_e S_e^{(i)}$ is equivalent to the share of each element's dissipation energy.

E. Conversion to Normal Coordinates of Nonlinear Discretization Equations

The equation of motion described with physical coordinates in (6) has large degrees of freedom, and hence, the calculation

time increases substantially. Therefore, normal coordinates corresponding to the linear normal vibration mode are introduced into (6) to reduce the degrees of freedom [3]–[5]. Here, the linear normal vibration mode $\{\phi^{(i)}\}$ closely resembles $\{\phi^{(i)}\} \cong \{\phi^{(i)}\}_0$ by $\{\phi^{(i)}\}_0$ of Section 3.D. By introducing the normal coordinate $\tilde{b}_i$ corresponding to this $\{\phi^{(i)}\}_0$, we can express displacement $\{U\}$ as the following equation:

$$\{U\} = \sum_{i=1} (1/n_i)\, \tilde{b}_i \{\tilde{\phi}^{(i)}\}_0 \tag{13}$$

Here, $\{\phi^{(i)}\}_0 = \{\tilde{\phi}^{(i)}\}_0 / n_i$, $m_i = \{\phi^{(i)}\}_0{}^T [M] \{\phi^{(i)}\}_0$, $n_i = (m_i)^{-(1/2)}$, $\{\tilde{\phi}^{(i)}\}_0{}^T [M] \{\tilde{\phi}^{(i)}\}_0 = 1$. By substitution of (13) into (6) and applying the normal coordinates, we can obtain the nonlinear simultaneous third-order ordinary differential equation.

$$M(\tilde{b}_i) \equiv \ddot{\tilde{b}}_i + \eta_{tot}{}^{(i)} \omega_0{}^{(i)} \dot{\tilde{b}}_i + (\omega_0{}^{(i)})^2 \tilde{b}_i + \sum_j \sum_k \tilde{D}_{ijk} \tilde{b}_j \tilde{b}_k + \sum_j \sum_k \sum_l \tilde{E}_{ijkl} \tilde{b}_j \tilde{b}_k \tilde{b}_l \tag{14}$$

$(i, j, k, l = 1,2,3,...)$

where $\tilde{P}_i = n_i \{\tilde{\phi}^{(i)}\}_0{}^T \{F\}$,

$$\tilde{D}_{ijk} = \sum_{m=1} \gamma_{2mz} (n_i / (n_j n_k)) \tilde{\phi}_{amzi} \tilde{\phi}_{amzj} \tilde{\phi}_{amzk},$$

$$\tilde{E}_{ijkl} = \sum_{m=1} \gamma_{3mz} (n_i / (n_j n_k n_l)) \tilde{\phi}_{amzi} \tilde{\phi}_{amzj} \tilde{\phi}_{amzk} \tilde{\phi}_{amzl},$$

$$\{\tilde{\phi}^{(i)}\}_0 = \{\tilde{\phi}_{1Xi}, \tilde{\phi}_{1Yi}, \tilde{\phi}_{1zi}, \tilde{\phi}_{2Xi}, \tilde{\phi}_{2Yi}, \tilde{\phi}_{2zi}, \tilde{\phi}_{3Xi}, ...\}^T.$$

$\tilde{\phi}_{amzi}$ is the z component of $\{\tilde{\phi}^{(i)}\}_0$ in the connecting node of α_m the nonlinear spring and the diaphragm center section. Equation (14) has substantially reduced degrees of freedom in comparison with (6).

IV. Resonance Frequency and Normal Modes

Resonant frequencies and normal modes were obtained and compared through an eigenvalue analysis. The main results are shown in Fig. 3. Modes 1 and 2 are resonant modes of the translational motion in the x and y directions. Modes 3–5 are the resonant modes of the rotation for the x, y, and z axial center of the center section. Mode 6 is the expansion and contraction of the nonlinear concentrated spring in the z direction, the main resonant mode. Modes 7 and 8 are the resonant modes of the saddle-shaped elastic deformation. Mode 9 is the resonant mode of the elastic deformation of the plate vibration. Modes 10 and 11 are the resonant modes of the higher order elastic deformation of the plate vibration. Modes 12 and 13 are the resonant modes of the relatively high-order saddle-shaped elastic deformation. Modes 14 and 15 are the resonant modes of the higher order elastic deformation of the plate vibration.

V. Linear Vibration Characteristics

A small external excitation force $\tilde{P}_i$, which is represented by a triangular pulse shown in Fig. 4, was applied to the excitation point. The spectrum of the response to this small input condition, which is a linear frequency response curve, shows the basic characteristics of the system. The time history of the displacement at an observation point was obtained by the fourth-order Runge–Kutta–Gill method. The spectrum shown in Fig. 5 was obtained by a Fourier transformation of the time history. The horizontal axis denotes the analytic frequency $\omega_{sp}/2\pi$, and the vertical axis denotes the spectral amplitude in decibel value A ($\omega_{sp}/2\pi$). The mode numbers are shown in parentheses. From this, it can be seen that nonlinear concentrated springs show large amounts of deformation, expressed as high peaks in the spectral amplitude, in Modes 4 and 5 (rotation about the x- and y-axes), Mode 6 (piston motion), Mode 9 (elastic deformation of the plate vibration) and Modes 10 and 11 (higher order elastic deformation of the plate vibration). In addition, Modes 7 and 8 (saddle-shaped elastic deformation) and Modes 14 and 15 (higher order elastic deformation of the plate vibration) have appeared slightly.

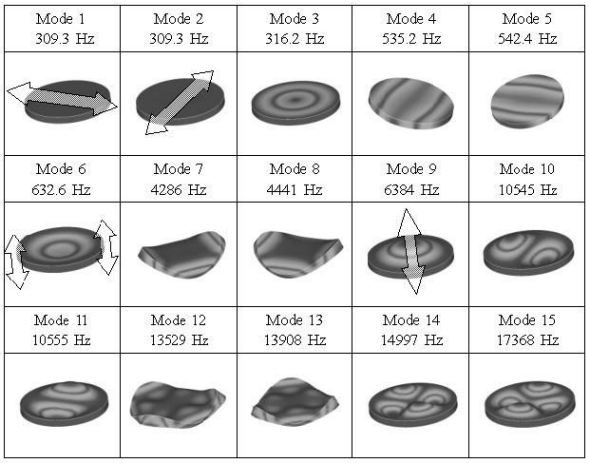

Fig. 3 Vibration modes of eigenvalue analysis

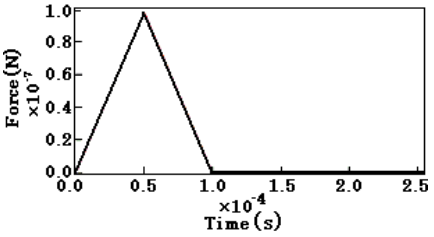

Fig. 4 Small input of impact load

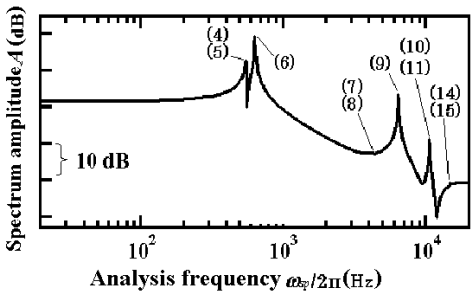

Fig. 5 Fourier spectrum of impact response under small input

An examination of this small impact revealed that under large input forces, a nonlinear response owing to nonlinear concentrated springs and various types of nonlinear mode coupling occurs.

VI. Nonlinear Steady-State Response to Harmonic Input

A. Nonlinear Transient Response

Under the condition of large input forces, responses become nonlinear, and nonperiodic responses such as chaotic vibrations may appear. In such cases, it is necessary to seek a direct integration solution. In (14), $\tilde{b}_i = b_i^{(1)}$, and its velocity $b_i^{(2)}$ is $\dot{\tilde{b}}_{(i)}$. Further, a harmonic input of excitation angular frequency ω is applied. By using the maximum approximate mode number I_c, we convert the following first-order simultaneous ordinary differential equation into a state equation.

$$\dot{\tilde{b}}_i^{(1)} = b_i^{(2)} \tag{15}$$

$$\dot{\tilde{b}}^{(2)} = -\eta_{tot}^{(i)}\tilde{\omega}_i\dot{\tilde{b}}_i^{(1)} - \tilde{\omega}_i^2\tilde{b}_i^{(1)} - \sum_j\sum_k \tilde{D}_{ijk}\tilde{b}_j^{(1)}\tilde{b}_k^{(1)}$$

$$-\sum_j\sum_k\sum_l \tilde{E}_{ijkl}\tilde{b}_j^{(1)}\tilde{b}_k^{(1)}\tilde{b}_l^{(1)} + P_{di}\cos\omega t \tag{16}$$

The integration of (16) directly with the fourth-order Runge–Kutta–Gill method solves the problem of the time history of the response and calculates the behavior of the solution in the phase.

B. Computational Conditions

This section examines the mode coupling of the coupled chaotic vibration behavior of the main mode (Mode 6) of the deformation of the nonlinear concentrated springs in the z direction with Modes 4,5 and Modes 7,8. Computations were carried out under the following condition: changing the excitation force under a fixed excitation frequency. As an excitation condition, the diaphragm can be easily inclined because the lead wire adheres to the diaphragm; hence, the fact that the input may easily become uneven was considered. A load, within a suitable width range, was added to the node on the electric conductor where the lead wire was glued. The response reference point was set in the central vicinity of the diaphragm.

C. Nonlinear Chaotic Vibration Response

A nonlinear chaotic vibration response, with a varying excitation force at an excitation frequency fixed at the natural frequency 632.6 Hz of Mode 6, which is a large deformation of the nonlinear concentrated spring, was computed. Fig. 6 shows the results, with time histories on the left-hand side and Fourier spectrums on the right-hand side. The vertical axis, u (mm), of the time histories represents displacement, and the horizontal axis, t (s), denotes time. The horizontal axis of the Fourier spectrums denotes the analytic frequency $\omega_{sp}/2\pi$ Hz, and the vertical axis denotes A ($\omega_{sp}/2\pi$) dB of the spectrum amplitude. In the case of a small exciting force p_{di} = 6.76e-7, the time history shows a linear periodic response that approximately corresponds to the excitation frequency. In the Fourier spectrum, only the component of excitation frequency exists. When the excitation force becomes p_{di} = 6.76e-3, in the Fourier spectrum, the component of excitation frequency and the harmonic components of integer times ($\omega^{(6)}$, $2\omega^{(6)}$, $3\omega^{(6)}$, …) are excited to a component six times the excitation frequency. When the excitation force becomes p_{di} = 6.76e-2, in the time history, a beating phenomenon occurs and a non-steady-state response is generated. In the Fourier spectrum, the component of excitation frequency and the harmonic components ($\omega^{(6)}$, $2\omega^{(6)}$, $3\omega^{(6)}$, …) of integer times are observed. Furthermore, in nonlinear coupling, Mode 9($\omega^{(9)}$), Modes 10 and 11($\omega^{(10)}$,$\omega^{(11)}$), and Modes 7 and 8($\omega^{(7)}$,$\omega^{(8)}$) are excited, and a harmonic wave response with the components of the fractions of the excitation frequency, 1/n (n: integer), ($\omega^{(7)}/2$, $\omega^{(8)}/2$, $\omega^{(9)}/2$, $\omega^{(10)}/2$, $\omega^{(11)}/2$, $\omega^{(7)}/3$, $\omega^{(8)}/3$, $\omega^{(9)}/3$, …) is also excited. The result shows several comparatively large peaks in the spectrum, with the internal resonance occurring around 2,000 Hz ($3\omega \cong 3\omega^{(6)} \cong \omega^{(7)}/2 \cong \omega^{(8)}/2 \cdots$) with multiple peaks and new peaks occurring in zones different from the excitation frequency and the linear resonance frequencies. Further, from the internal resonance, a discontinuous rotation with the vibration modes of revolution about the x- and y-axes (Modes 4 and 5) is also induced. As a result, the width of the small vibrating components (side band) is clearly visible.

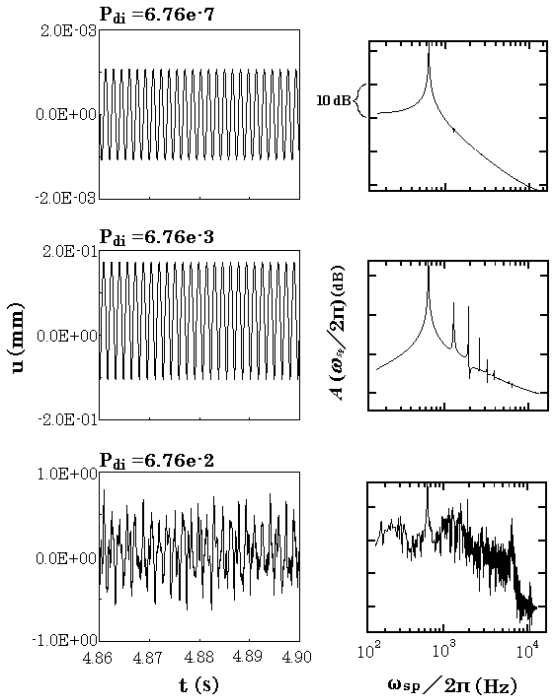

Fig. 6 Time response curve and Fourier spectrum

Based on this characteristic, the transient vibration is likely to be a chaotic vibration. The nonlinear mode coupling between the diaphragm center section and the nonlinear spring was inspected, and the following results were obtained:

(1) The vibration mode of rotation about the x-axis and the y-axis had a 1:1 internal resonance relationship.

(2) The two vibration modes of the saddle-shaped elastic deformation had a 1:1 internal resonance relationship.

(3) The two vibration modes of the higher order elastic deformation of the plate vibration had a 1:1 internal resonance relationship.

The chaotic vibration was attributed to the coupling of multiple internal resonances. Furthermore, based on the simulation model, the piston motion vibration mode, in which the deformation of the nonlinear concentrated springs was large, and the vibration mode of saddle-shaped elastic deformation had a 1:7 internal resonance relationship. Moreover, with respect to the vibration modes of rotation about the x- and y-axes, the vibration modes of the saddle-shaped elastic deformation had a 1:8 internal resonance relationship. Moreover, the piston motion vibration mode and the elastic deformation of the plate vibration of the center section had a 1:10 internal resonance relationship. Thus, these vibrations, coupled with the internal resonances (1), (2), and (3) described in the preceding paragraph, become chaotic vibrations.

D.Vibration Analysis by Lyapunov Exponent

Using Wolf's method [9], we calculated the largest Lyapunov exponent from the non-steady-state time history under the analytical condition of p_{di} = 6.76e-2 in Fig. 6, where the non-steady-state response appears. The result is shown in Fig. 7. The horizontal axis represents the embedded dimension e, and the vertical axis represents the largest Lyapunov exponent λ_{max}. The largest Lyapunov exponent λ_{max} with a positive value of approximately 0.04 was obtained. Hence, the transient vibration can be determined as a chaotic vibration. The largest Lyapunov λ_{max} exponent became almost constant at 12 dimensions. Hence, the number of high modes contributing to the chaotic vibration was presumed to be six. Further, the analytical result under these conditions and, for comparison purposes, the animation data output of the time change in the displacement amplitude of the finite element model, under the analytical conditions of $\omega/2\pi$=632.6Hz, verified the circumstances that led to the nonlinear vibration response.

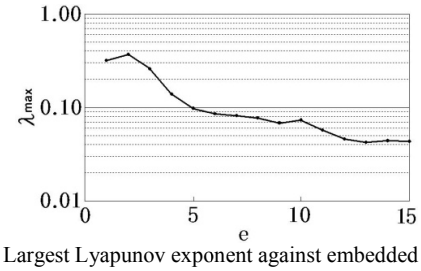

Fig. 7 Largest Lyapunov exponent against embedded dimension

Furthermore, snapshots were taken from the animation, which extracted pictures of features of the vibration modes that were thought to have occurred, as shown in Fig. 8. From the animation data in the case of p_{di} = 6.76e-7, we concluded that only Mode 6 appeared, but from the case of p_{di} = 6.76e-2, it was possible to observe six modes appeared.

VII. Conclusion

Using a finite element method, we carried out an analysis of a nonlinear vibration response for a system of a diaphragm center section connected to nonlinear springs. The nonlinear discretization equations were converted to equations of motion using normal coordinates corresponding to the linear vibration mode. Further, the degrees of freedom were reduced, and the response of a large-scale degree of freedom problem was analyzed at high speed. As an analytical condition, the nonlinear vibration and the chaotic vibration were calculated under special conditions for large external forces.

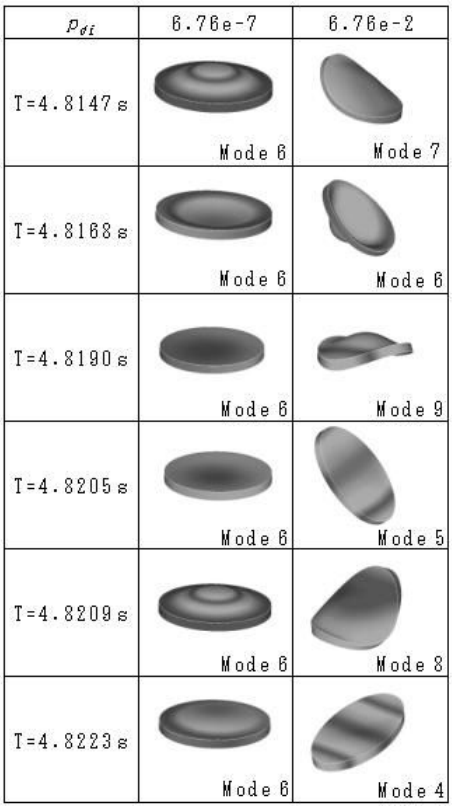

Fig. 8 Instantaneous distribution of deformation in chaotic motion

REFERENCES

[1] T. Kondo, T. Sasaki, and T. Ayabe, "Forced vibration analysis of a straight-line beam structure with nonlinear support elements," *Trans. Jpn. Soc. Mech. Eng.*, vol. 67, no. 656C, pp. 914–921, 2001.

[2] E. Pesheck, N. Boivin, C. Pierre, and S. W. Shaw, "Non-linear modal analysis of structural systems using multi-mode invariant manifolds," *Nonlinear Dyn.*, no. 25, pp. 183–205, 2001.

[3] T. Yamaguchi, K. Nagai, S. Maruyama, and T. Aburada, "Finite element analysis for coupled vibrations of an elastic block supported by a nonlinear spring," *Trans. Jpn. Soc. Mech. Eng.*, vol. 69, no. 688C, pp. 3167–3174, 2003.

[4] T. Yamaguchi, N. Nakahara, K. Nagai, S. Maruyama, and Y. Fujii, "Frequency response analysis of elastic blocks supported by a nonlinear spring using finite element method," *Trans. Jpn. Soc. Mech. Eng.*, vol. 70, no. 696C, pp. 2219–2227, 2004.

[5] T. Yamaguchi, T. Saito, K. Nagai, S. Maruyama, Y. Kurosawa, and S. Matsumura, "Analysis of damped vibration for a viscoelastic block supported by a nonlinear concentrated spring using FEM," *J. Syst. Des. Dyn.*, vol. 4, no. 1, pp. 154–165, 2011.

[6] E. H. Dowell, "Flutter of a buckled plate as an example of chaotic motion of a deterministic autonomous system," *J. Sound Vib.*, vol. 85-3, pp. 333–344, 1982.

[7] A. H. Nayfeh and R. A. Raouf, "Nonlinear Forced Response of Infinitely Long Circular Cylindrical Shells," *J. Appl. Mech.*, vol. 54, pp. 571–577, 1987.

[8] X. L. Yang and P. R. Sethna, "Non-linear phenomena in forced vibrations of a nearly square plate: Antisymmetric case," *J. Sound Vib.*, vol. 155-3, pp. 413–441, 1992.

[9] A. Wolf, J. B. Swift, H. L. Swinney, and J. A. Vastano, "Determining Lyapunov exponents from a time series," *Physica*, vol. 16D, pp. 285–317, 1985.

[10] O. C. Zienkiewicz and Y. K. Cheung, *The Finite Element Method in Structural and Continuum Mechanics.* New York: MacGraw-Hill, 1967.